J. Fluid Mech. (2000), *vol.* 405, *pp.* 37–56. Printed in the United Kingdom

The electrohydrodynamic stability of a liquid bridge: microgravity experiments on a bridge suspended in a dielectric gas

By C. L. BURCHAM† AND D. A. SAVILLE

Department of Chemical Engineering, Princeton University, Princeton NJ 08544, USA

(Received 20 July 1998 and in revised form 7 October 1999)

The electrohydrodynamic stability of a liquid bridge was studied in steady and oscillatory axial electric fields with a novel apparatus aboard a space shuttle. To avoid interphase transport, which complicates matters in terrestrial, matched-density systems, the experiments focused on a liquid column surrounded by a dielectric gas. The micro-gravity acceleration level aboard the spacecraft kept the Bond number small; so interface deformation by buoyancy was negligible. To provide microgravity results for comparison with terrestrial data, the behaviour of a castor oil bridge in a silicone oil matrix liquid was studied first. The results from these experiments are in excellent agreement with earlier work with isopycnic systems as regards transitions from a perfect cylinder to the amphora shape and the separation of an amphora into drops. In addition, the location of the amphora bulge was found to be correlated with the field direction, contrary to the leaky dielectric model but consistent with earlier results from terrestrial experiments. Next, the behaviour of a bridge surrounded by a dielectric gas, sulphur hexafluoride (SF_6), was investigated. In liquid–gas experiments, electrohydrodynamic ejection of liquids from 'Taylor cones' was used to deploy fluid and form bridges by remote control. Experiments with castor oil bridges in SF_6 identified the conditions for two transitions: cylinder–amphora, and pinch-off. In addition, new behaviour was uncovered with liquid–gas interfaces. Contrary to expectations based on perfect dielectric behaviour, castor oil bridges in SF_6 could not be stabilized in AC fields. On the other hand, a low-conductivity silicone oil bridge, which could not be stabilized by a DC field, was stable in an AC field.

1. Introduction

Electrohydrodynamics involves interactions between fluid motion and electrical fields, customarily with non-polar, low-conductivity liquids known as *leaky dielectrics*. Although their conductivities are small, often five to eight orders of magnitude less than tap water, such liquids must be treated as Ohmic conductors whenever free charge accumulates at a fluid interface (Taylor 1966). In an applied field, interfacial charge leads to tangential electric forces and fluid motion arises to provide a balancing stress. Perfect dielectric (insulating) behaviour is qualitatively and quantitatively different since free charge is absent and the electrical stress is always normal to the interface. Taylor proposed a methodology, now known as the Taylor–Melcher leaky dielectric model, to deal with situations involving fluid interfaces.

† Present address: Dow AgroSciences, L.L.C., Formulations Science and Technology, 9330 Zionsville Rd, Indianapolis, IN 46268, USA.

While qualitative predictions of the theory agree with experiments, the extent to which the leaky dielectric boundary condition provides an accurate representation remains to be demonstrated. Extensive drop deformation experiments with isopycnic systems by Torza, Cox & Mason (1971) and Vizika & Saville (1992) disclosed good agreement between theory and experiment with some liquid pairs and nagging discrepancies with others. Theoretical treatments of nonlinear aspects of the model (Feng & Scott 1996) provide new insights but have not resolved all the issues. The purpose of our experiments was to examine electrohydrodynamic behaviour where the interface boundary condition could be idealized as much as possible. This involved suspending bridges in a dielectric gas to eliminate charge transport across the interface.

The experiments reported here are of two sorts. First, microgravity experiments with liquid–liquid systems gave results consistent with those from earlier terrestrial investigations in matched-density systems. This provides assurance that the apparatus functioned in a manner consistent with that used in terrestrial work. Following this, experiments were carried out on castor oil and silicone oil bridges suspended in the dielectric gas sulphur hexafluoride, SF_6. Pure castor oil bridges were investigated at two different aspect ratios above the Plateau limit; behaviour at a single aspect ratio was studied with an enhanced-conductivity castor oil. The behaviour of a low-conductivity silicone oil was studied at a single aspect ratio above the Plateau limit. The behaviour encountered is both interesting and fascinating. With castor oil and enhanced-conductivity castor oil (each is a relatively high-conductivity liquid compared to silicone oil) it was possible to stabilize bridges above the Plateau limit using a DC field. Such behaviour is consistent the leaky dielectric model and with experiments on bridges in a matrix liquid. The cylinder–amphora transitions with the two castor oil systems were the same at a given aspect ratio, as expected from the leaky dielectric model for a bridge in a non-conducting gas. However, using AC fields oscillating at frequencies much higher than needed to nullify charge relaxation, castor oil bridges in SF_6 could not be stabilized above the Plateau limit. This is at odds with the leaky dielectric picture which, according to Torza *et al.* (1971), goes smoothly over to perfect dielectric behaviour when the frequency is high enough to nullify charge relaxation. Conversely, a bridge formed from a very low-conductivity silicone oil was stable in an AC field but unstable in a DC field. Behaviour of this sort is consistent with the perfect dielectric model only when the field oscillation frequency is well above the charge relaxation frequency. Our measurements on silicone oil indicated Ohmic behaviour with a conductivity about $\frac{1}{30}$th of castor oil and an electrical relaxation time of 24 s. The implications of these results and suggestions for future investigations will be discussed after the detailed results have been presented.

These experiments, the first on liquid bridges in a dielectric gas, provide evidence of interesting behaviour with 'perfectly reflecting' interfaces. Due to the unavoidable limitations imposed by working in the microgravity environment, it was not possible to explore as wide a variety of conditions as one would like. Nevertheless, the results reported here stem from repeated observations of the phenomena. Accordingly, the experimental data are reliable. It will be important to carry out further experiments with gas–liquid interfaces under less restricted conditions.

At present the most comprehensive results on liquid bridges deal with dynamics in the absence of electrical forces or pertain to their behaviour as perfect dielectrics. Zhang, Padgett & Basaran (1996) analyse the deformation and breakup of bridges and provide a comprehensive review of the literature on behaviour in the absence of external fields. A seminal series of papers by Castellanos' group at the Universidad

de Sevilla deals with perfect dielectric bridges in axial fields. Their first theoretical and experimental study (González *et al.* 1989) showed close agreement with AC fields, except near the Plateau limit where the length of the bridge is equal to its circumference. The discrepancies prompted follow-up theoretical studies on the effects of buoyancy (González & Castellanos 1993; Ramos & Castellanos 1993). New experimental results on the stability of cylindrical bridges (Ramos, González & Castellanos 1994) showed good agreement when the effects of buoyancy were included. Where possible, these results will be compared with the current experiments. Although a linearized theory has been worked out for leaky dielectrics in steady fields (Burcham 1998), it cannot address the qualitative issues raised here since it is based on the leaky dielectric premises. Dealing with these issues will require a more general theory and additional experiments.

2. Background

A central feature of the conceptual model is free charge accumulation at – and transport across – a liquid–liquid interface. Electric charge is carried by ions whose effective size is influenced by complexation with solvent molecules and, in apolar liquids, dynamic chemical equilibria between charged and uncharged entities may be involved. Thus, current flow through an interface is a complex sequence of events whereby ions shed solvent molecules of one phase and reconfigure themselves in the new phase. However, charge transport in apolar liquids is poorly understood; even less is known about how ions move near and across interfaces. Consequently, the leaky dielectric model simplifies matters by representing charge transport near the interface as an Ohmic process; charge accumulation within a material surface element is balanced by conduction from bulk fluid on either side of the surface. At steady state,

$$(\sigma E)_i = (\sigma E)_e \tag{1}$$

with (σE) denoting the current (the product of the conductivity, σ, and the field strength normal to the surface, E) on the side of the interface indicated by a subscript i for the interior or e for the exterior. This relationship sets the magnitudes of the fields and Gauss' law establishes the free-charge density, q, in terms of the dielectric constant, ε, of each fluid and the permittivity of free space, ε_o, namely

$$q = (\varepsilon_o \varepsilon E)_e - (\varepsilon_o \varepsilon E)_i = \varepsilon_o \varepsilon_i [\varepsilon_e/\varepsilon_i - \sigma_e/\sigma_i] E_e. \tag{2}$$

It is the free-charge density which determines the tangential electric stress and the intensity of electrohydrodynamic motion. For further details see Saville (1997).

Two issues arise in connection with the boundary condition embodied in (1). First, the simple conduction model may not represent interphase transport adequately as ions move between phases. Second, as noted, the conductivities of leaky dielectrics are low and therefore sensitive to contamination. One way of addressing these issues experimentally is to avoid interphase transport altogether by immersing a leaky dielectric liquid body in a non-conducting, dielectric gas. Of course the body must be in contact with electrodes to provide sources of free charge. This provides a non-conducting boundary and the Ohmic conductivity parameter disappears from the theoretical model. Now, according to (2), the interface free-charge density depends only on dielectric properties. The boundary condition for current becomes 'perfectly reflecting' with no flux across the surface. However, free charge still accumulates on the interface whenever it is not aligned with the field and this provides electric stresses,

which must be balanced by flow. The surviving electrical parameters are dielectric constants, which are insensitive to contamination and readily measured. Coupling between electrostatics and hydrodynamics occurs through the Maxwell and viscous stresses and interfacial tension at the gas–liquid interface.

To focus on behaviour without interphase transport, we carried out experiments using a liquid bridge suspended in the dielectric gas, SF_6. The liquid bridge configuration, albeit without electrical effects, has been the focus of research dating from the 19th century work of Plateau (1863, 1864, 1865, 1866). He showed that, provided gravitational effects are negligible, a bridge is stable if its length, l, is less than its circumference, $2\pi a$. In Plateau's work, buoyancy was suppressed by immersing the body under study in an immiscible liquid of the same density. This isopycnic arrangement has been utilized in electrohydrodynamics by González *et al.* (1989) and Sankaran & Saville (1993), who studied the stabilizing effects of an axial electric field. With a liquid bridge the situation is as follows. When the bridge spanning the two electrodes is cylindrical, the electric field inside and outside the column is uniform and the interface is charge free. Should the bridge deform, charge is induced on a leaky dielectric. An axial field can stabilize a liquid cylinder whose aspect ratio, $\beta \equiv l/2a$, is above the Plateau limit, π, irrespective of whether it behaves as a perfect (non-conducting) or leaky dielectric. However, when the liquid responds as a leaky dielectric, the required field strength is much less due to the presence of free charge. Saville (1997) reviews the current state of affairs.

We utilized the microgravity environment of NASA's space shuttle *Columbia* during the Life and Microgravity Spacelab Mission (STS-78, June 20–July 7, 1996) to suppress buoyancy. In the absence of gravity, the compromising effects of the outer liquid of the Plateau configuration are avoided and a 'perfectly reflecting' boundary secured. Because the space shuttle apparatus operates where the effective gravitational acceleration is five orders of magnitude less than the terrestrial level, the Bond number,

$$B_0 = \frac{g(\rho_i - \rho_e)a^2}{\gamma}, \tag{3}$$

can be kept small without matching densities. Here the gravitational acceleration is represented by g, densities of the bridge and surrounding fluid by ρ_i and ρ_e, interfacial tension by γ, and the undeformed radius by a. In our work where the bridge was surrounded by a dielectric gas, the Bond number for millimetre-size objects was $O(10^{-4})$ for a surface tension of $10\,\mathrm{mN\,m^{-1}}$. As a result, gravitational deformation was negligible.

The presentation is organized as follows. The apparatus configuration is described first, including the features used to acquire images of the bridge. Then the experimental procedures are outlined including the methodology for forming bridges in orbit. Following this, experiments with a two-phase system using fluids similar to those employed in terrestrial experiments are described. The results show that the apparatus functioned in a manner consistent with that used earlier and was free of anomalies. The paper concludes with a discussion of extensive experiments with liquid bridges suspended in the dielectric gas, SF_6.

3. Apparatus design

In conceptual terms, the experiments are quite simple. The bridge, a liquid column held between parallel plates with pinned contact lines, is depicted in figure 1. To stabilize the bridge above the Plateau limit, an axial field is created by applying

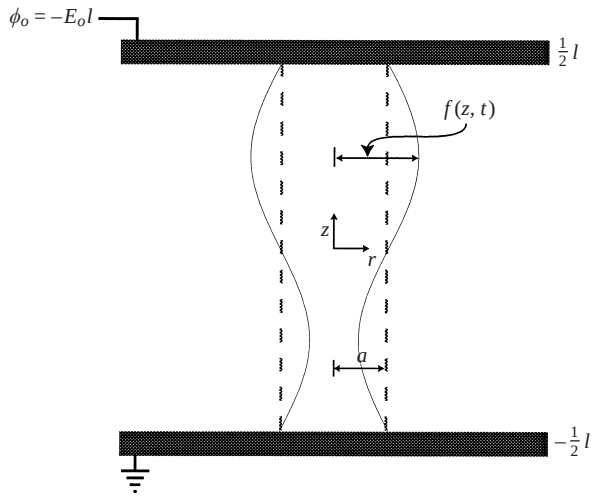

FIGURE 1. A sketch of a liquid bridge of length l. The undeformed bridge of radius a is indicated by a dashed line; solid lines represent the deformed interface, $f(z, t)$.

voltage to one plate while grounding the other. When the field strength is high, the bridge is cylindrical and quiescent. Upon lowering the field strength two transitions are encountered: (i) from cylinder to amphora and (ii) separation into two drops (pinch off). In the amphora configuration a steady flow is set up to help balance the stress; a steady electric field can maintain the amphora configuration indefinitely. After the bridge has broken, increasing the field causes the bridge to re-form with an amphora shape. Images of a bridge at different stages of deformation and field strengths are recorded to characterize behaviour.

Our liquid bridge experiments were performed onboard the space shuttle in the Bubble Drop and Particle Unit (BDPU) facility. The BDPU, owned by the European Space Agency (ESA), is a self-contained, multi-purpose fluid physics unit accommodating different experiments. The BDPU provides the necessary support equipment in terms of computer control and data acquisition, power, thermal control, and video and telemetry downlinks. Each BDPU experiment is carried in a $22\,\text{cm} \times 41\,\text{cm} \times 25\,\text{cm}$ module known as a test container. Plester (1997) gives a detailed description. Dornier Aerospace (Friedrichshafen, Germany) was the prime contractor for our experiment and the test containers were constructed under subcontracts. Ferrari S.p.A. (Modena, Italy) designed, built, and assembled the mechanical hardware including the test container housing, experimental cells, and systems employed to pump fluids and move elctrodes. Laben S.p.A. (Milan, Italy) was responsible for the electronics and control systems, along with integration of the electrical components with the mechanical hardware from Ferrari. Alenia Spazio, (Turin, Italy) handled the computer links between the BDPU and the test container. Trek (Medina, New York) and Teledyne Brown Engineering (Huntsville, Alabama) developed the high-voltage power supply, controlled by the logic interface assembly furnished by Laben.

Our design incorporates three experimental cells per test container: two for single-phase experiments and one for two-phase experiments. Each cell is mounted on a carousel to align it with the windows of the test container. In turn, the windows line up with cameras to provide two orthogonal views of the cell. Temperature control is through a Peltier heat exchanger mounted on the back of the test container using

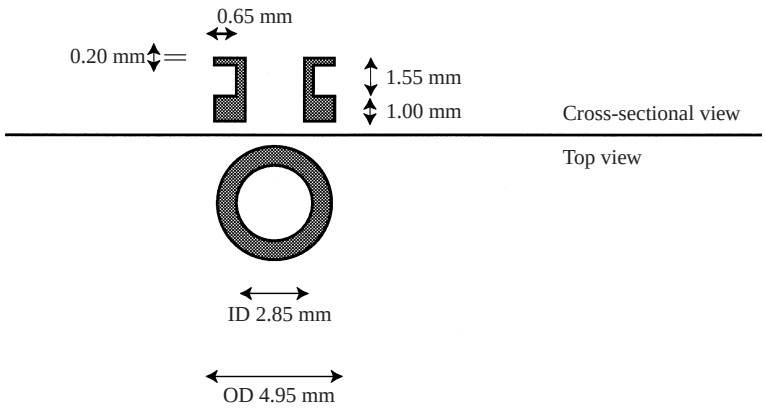

FIGURE 2. Containing rings. Note the 1 mm counter-sink into the electrode.

air provided by the cooling duct of the BDPU. Thermocouples located throughout the test container ensure a uniform temperature. During our experiments the average temperature was 22.6 °C.

Each cell is equipped with circular, 314 stainless steel electrodes (3.7 cm, diameter), polished to a mirror finish with rounded edges. The maximum electrode separation is 5 cm. Finite-element calculations show that the effect of the outer (glass) containment is negligible so, as a first approximation, we can regard the bridge as situated between infinite plates. Delrin® ($\varepsilon = 3.8$) containing rings with a grooved geometry (figure 2) are used to pin the contact lines of the liquid bridge to the electrodes. Each ring is centred on an electrode.

To ensure alignment of the bridge, the containing rings are concentrically embedded in the electrodes (figure 2). Although the rings and the countersink geometry perturb the electrical field near the liquid contact line, the effect is believed negligible; finite-element calculations carried out by Dornier Aerospace show that the scale of the perturbation is small. No unusual activity, e.g. flow, was ever observed near the contact lines. Fluorad® Fluorochemical Coating FC-722 (3M Corporation), an anti-wetting material, is used to treat the surface of the electrodes outside the containing rings in single-phase cells.

The electrodes and the liquid bridge are located inside octagonal, quartz glass cells. The four walls in line with the cameras are optically clear; the others have a rough 'frosted' surface to avoid stray reflections. Most of the apparatus is constructed of Torlon® and Peek® because of their favourable structural properties. Viton® O-ring seals are used. Since electrical discharge must be avoided, single-phase cells are filled with SF_6. SF_6 is a well-known, high-breakdown-strength inert gas ($\varepsilon = 1.00$) that is difficult to ionize and is therefore used in the electronics industry as an insulator. The gas in the cells is at atmospheric pressure; test containers are filled with SF_6 diluted with nitrogen. Accordingly, ionization in the cells and test containers was suppressed.

The BDPU is designed for remote operations from the Payload and Operations Control Center (POCC) at Marshall Space Flight Center, Alabama, with limited interactions from the shuttle crew. The test container is controlled through commands sent to the BDPU. In addition to housing the 'commanding' hardware, the BDPU collects data that are downlinked to the POCC. During the mission, telemetry data is displayed with a LabVIEW® program written by the Microgravity Advanced Research

and Support Center – MARS (Naples, Italy). The program, named the MMI (or Man Machine Interface), converts the downlinked data into a useful format and displays it graphically on a computer monitor. The MMI program was also used post-mission to analyse the recorded mission data.

4. Experimental procedures

4.1. *Bridge formation*

For each experiment, a liquid column must be formed. In two-phase experiments, a short bridge (~ 1 mm) was prepared during assembly of the test containers prior to the launch. For single-phase experiments, bridges were formed in orbit to avoid spilling fluid from the containing rings during launch. We used a Taylor cone procedure developed during earlier flights on NASA aircraft (Pletser, Burcham & Cronise 1995) executing a 'parabolic trajectory' to mimic low-gravity conditions similar to those aboard an orbiting spacecraft. The first step in the Taylor cone procedure is to inject a drop of fluid into the containing ring on the fixed electrode using the remote control features of the apparatus. Next, the movable electrode is positioned 1.5 cm above the fixed electrode. Applying a steady (DC) 12 kV potential deforms the drop into a Taylor cone. Due to the high potential, fluid is ejected from the tip of the cone towards the movable electrode and collects inside the containing ring. During ejection from the fixed electrode containing ring, additional fluid is pumped in until the containing ring on the movable electrode is filled and a drop of fluid visible. Then the field is turned off and the electrodes moved until the drops coalesce. From this point, single-phase and two-phase experiments proceed in essentially the same fashion. The aspect ratio of the bridge can be altered by changing the movable electrode position while injecting or withdrawing fluid to maintain the bridge. Further details are given in Burcham (1998).

Following formation of a short bridge, the aspect ratio is increased until it is close to the Plateau limit, π, the volume of the bridge checked, and fluid added or withdrawn as necessary to ensure a 'perfect' cylinder using the image analysis system. Then, the aspect ratio is increased using an electric field to maintain a stable configuration while adding fluid as the electrode separation increases. Once the desired aspect ratio is reached and the bridge is cylindrical, the electric field is lowered in small steps to locate the cylinder–amphora transition and the pinch-off point. Between voltage steps, the bridge is allowed to assume a (new) steady-state configuration. Steady state is determined using a real-time image analysis program detailed in the following section but, in every case, more than 3 minutes were allowed to elapse to ensure a steady state. Once steady state is achieved, the voltage is lowered again and the process repeated. In some experiments, the sequence was reversed: starting from separate drops, coalescence and then the amphora–cylinder transition were identified. Thus, there are two transitions as the field is increased: coalescence and amphora–cylinder and two more as the field is lowered: cylinder–amphora and pinch-off. As expected, hysteresis is present, i.e. the amphora–cylinder and cylinder–amphora transitions occur at different field strengths. This is due to differences in the internal circulation patterns.

Following the mission, the high-voltage power supply was recalibrated to verify the data. None of the calibrations changed indicating that the data collected during the mission are reliable.

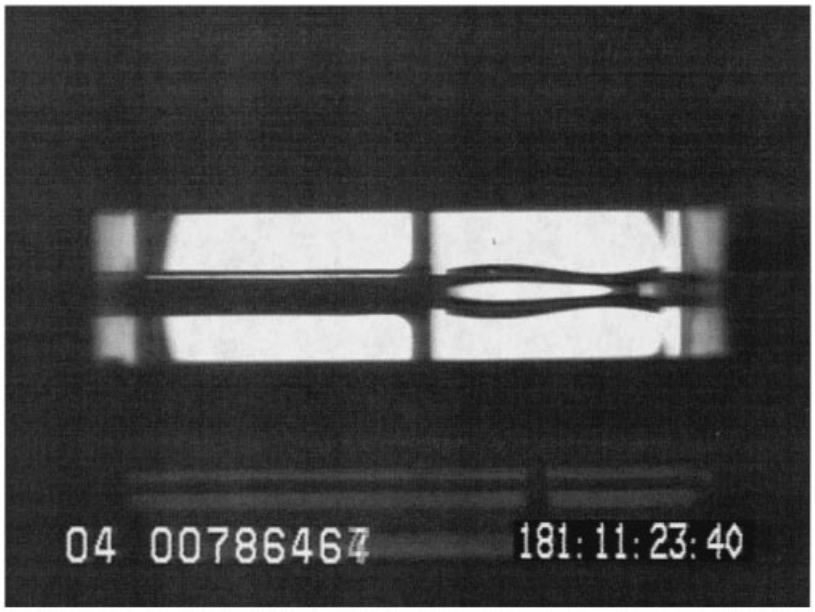

FIGURE 3. Image from the downlinked video.

4.2. *Image analysis*

Information about the configuration of the liquid bridge is derived from video signals transmitted from two CCD cameras mounted in line with ports in the test container. To analyse the shape of the bridge (figure 3), the video signal is directed to an image analysis system, consisting of a Power Macintosh® 9500/132 computer with 128 Mbytes of RAM and a PDI HMI-1 framegrabber to digitize the images. The images were analysed with a LabVIEW program written by MARS. The LabVIEW program utilized the Concept. VI Level II version 3.1 Image Processing and Analysis Tools package from Graftek Imaging.

The image analysis software produces an array of 'edge coordinates' from which an outline of the bridge can be constructed (figure 4). The edge coordinates are found by digitizing the image, applying a threshold, and scanning across the interface to locate the transition from 'light' to 'dark' pixels. The edge coordinates are also used with a fast Fourier transform (FFT) algorithm (see Press *et al.* 1992) to compute the first few complex Fourier coefficients of the interface position. The FFT coefficients are simply a set of complex numbers computed from the original data and can be used, therefore, to 'reassemble' the original data and interpolate between the data points. Changes in the magnitudes of the coefficients provide a sensitive numerical measure of the change in the interface. For example, after a steady-state configuration is established, the voltage is lowered, and shape changes monitored by following the evolution of FFT coefficient magnitudes and maximum or minimum radii. This is illustrated in figure 5, which shows changes in the bridge shape after the voltage is lowered. Figure 5(*a*) depicts the evolution of the maximum radius as a function of time and Figure 5(*b*) traces the evolution of the magnitudes of the first two FFT coefficients. As the bridge deforms, the first FFT coefficient magnitude grows, as does the maximum radius. In the figure, the maximum radius appears to change in discrete increments due to the resolution of

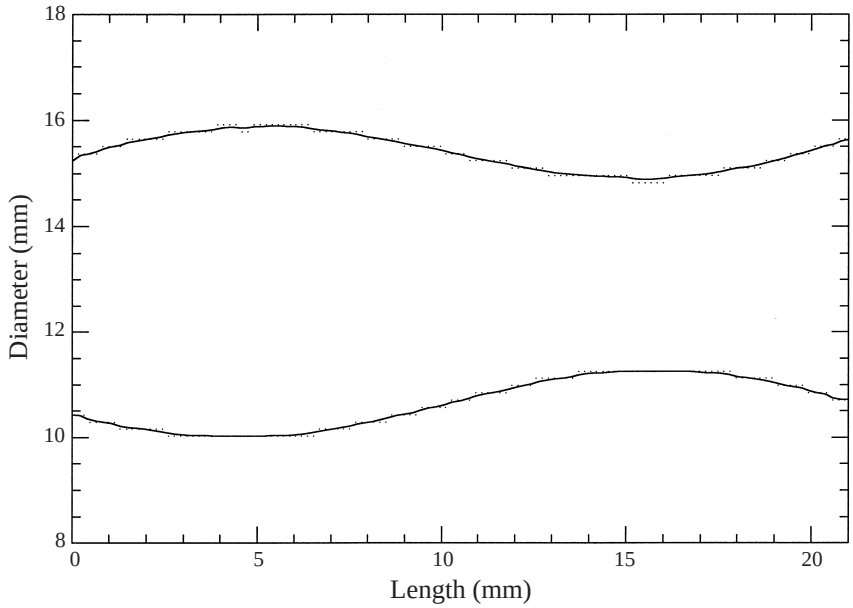

FIGURE 4. A reconstructed interface. The dots indicate the image points used to construct the smoothed image.

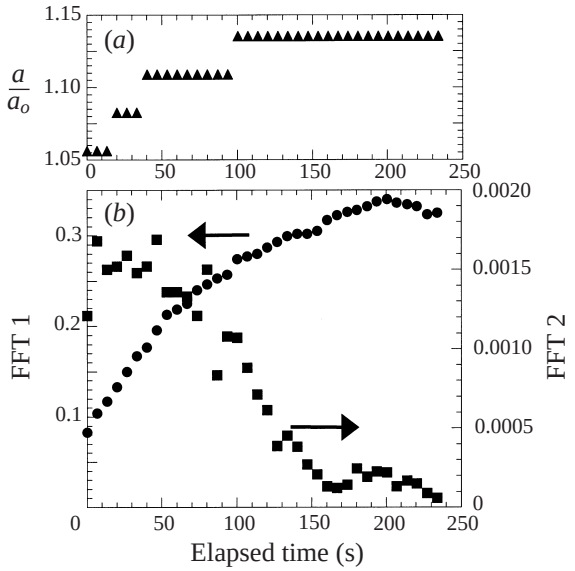

FIGURE 5. Behaviour of (*a*) the maximum radius and (*b*) the first (●) and second (■) fast Fourier transform coefficients after lowering the field.

the digitized image; each 'step' in the graph corresponds to one pixel (approximately 160 μm). However, the FFT coefficients change in a more continuous manner since they involve the positions of many points along the interface and thereby interpolate between pixel locations. Steady state is determined when the FFT coefficients no longer change with time. Usually this took less than 3 minutes. The ability to perform real-time image analysis and calculate FFTs proved critical during the experiment

since the FFT coefficients are quite sensitive to small changes in the bridge shape. This is readily seen during the time interval after 100 s in the figure. The maximum radius measurement suggests that steady state was reached at 100 s. However, the FFT coefficients show that steady state was not achieved until nearly 200 s had elapsed. The FFT coefficients were used to determine when a new steady-state configuration was achieved in the manner outlined above. They were also used in the analysis of the data to determine when an amphora–cylinder transition or pinch-off occurred. The amphora–cylinder transitions determined using the FFT data were the same as those found using the maximum and minimum radius.

In this work, interest centres on transitions – (i) from cylinder to amphora and vice versa and (ii) pinch-off. The cylinder–amphora transition is of particular interest since it should be amenable to calculation from a linearized hydrodynamic stability theory. Predicting the other transitions may require nonlinear methods. In the following sections the scaled maximum radius is used to indicate behaviour since it provides a simple, easily visualized indicator. However, all the transitions were identified using the full bridge shape from the image analysis system.

5. Experimental results

We utilized two test containers, with three experimental cells each, during the LMS mission. Each test container was used over separate 24-hour periods. The experiments dealt with the behaviour of single- and two-phase bridges in steady (DC) and sinusoidal (AC) electric fields. Some experiments were unsuccessful due to spilling of the bridge from the containing ring. However, successful runs were completed with both liquid–liquid and liquid–gas cells. Experimental results on the stability of a bridge in a matrix liquid in steady and AC electric fields are presented first, followed by the results with single-phase systems.

Experimental fluids were chosen based on a number of criteria. Obviously, the properties should be as different as possible from those in terrestrial experiments to exploit the microgravity environment. However, some tie-in with ground-based work is necessary to validate the microgravity experiments. Aside from properties such as viscosity, interfacial tension, conductivity and dielectric constant, the control parameters in a given experiment are the aspect ratio, β, and the ratio of electrical and interfacial tension forces, Δ, defined as

$$\beta \equiv \frac{l}{2a} \quad \text{and} \quad \Delta \equiv \frac{a\varepsilon_i\varepsilon_o E^2}{\gamma} \tag{4}$$

respectively; E denotes the axial field strength. The axial field was calculated from the voltage across the electrodes and the separation, allowing for the containing rings. For a given fluid system, the shape of the bridge depends on β and Δ. Some AC experiments were done using a frequency greater than the inverse electrical relaxation time. The electrical relaxation time, τ_e, follows from the dielectric constant and conductivity as

$$\tau_e = \frac{\varepsilon\varepsilon_o}{\sigma}, \tag{5}$$

where σ is the electrical conductivity. For AC experiments, the root-mean-square value of the electric field (E^2_{RMS}) was used and (Δ_{RMS}) was defined as

$$\Delta_{RMS} \equiv \frac{a\varepsilon_i\varepsilon_o E^2_{RMS}}{\gamma}. \tag{6}$$

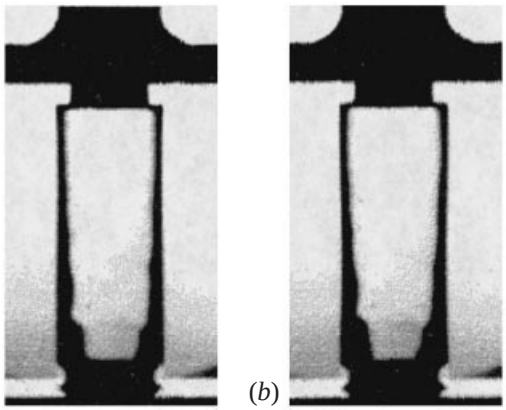

FIGURE 6. Castor oil/eugenol bridge in silicone oil 12 M, $\beta = 2.93$. (*a*) Without a field, (*b*) with a small field $\Delta = 0.007$.

Fluid	Density ($kg\,m^{-3}$)	Viscosity ($kg\,m^{-1}\,s^{-3}$)	Conductivity (Siemens m^{-1})	Dielectric Constant	τ_e (s)
Silicone Oil 12 M	973.0	11.79	1.98×10^{-12}	2.74	10
Castor Oil/Eugenol	972.6	0.372	2.42×10^{-9}	5.24	0.0191
Castor Oil	958.2	0.656	3.54×10^{-11}	4.65	1.16
High σ Castor Oil	958.3	0.631	1.67×10^{-9}	4.62	0.0245
Silicone Oil 1 M	972.6	0.977	1.00×10^{-12}	2.75	24.3
SF_6	5.97	1.576×10^{-5}	0.0	1.0	—

TABLE 1. Physical properties of the experimental fluids at 25 °C and 1 Atm.

Table 1 contains the physical properties of the fluids as measured in our laboratory (Burcham 1998). All the liquids behaved as Ohmic conductors at the high field strengths employed here. The interfacial tension, γ, of the castor oil/eugenol–silicone oil system is $13.07\,mN\,m^{-1}$, for castor oil in air $\gamma = 35.75\,mN\,m^{-1}$, and for silicone oil 1 M in air $\gamma = 21.3\,mN\,m^{-1}$.

5.1. *A castor oil/eugenol bridge in silicone oil*

A two-phase, nearly isopycnic, system was used first to validate the apparatus and provide a tie-in with the work of Sankaran & Saville (1993). Behaviour at two aspect ratios was examined, one below the Plateau limit and one above. As expected, a bridge with $\beta = 2.93$ was stable without a field and did not change shape when a small field was applied ($\Delta = 0.007$, figure 6). The gradations in the images are due to the somewhat uneven test container lighting. Image analysis indicates that the bridges in figures 6(*a*, *b*), 10(*a*, *b*), 11(*d*), and 13(*a*, *b*) are cylindrical to within the limits of detection. No attempt was made to form bridges in the absence of an electric field nearer to the Plateau limit due to time limitations.

Starting with an intact bridge below the Plateau limit, the aspect ratio was increased using a field to stabilize the bridge. Figure 7 depicts steady-state shapes of the bridge at different values of Δ; figure 8 depicts the maximum radius of the bridge, scaled by the undeformed radius, plotted against the dimensionless field strength, Δ. The experimental sequence is from left to right in figure 8. The points labelled *a*, *b* and *c* correspond to the images in figure 7. The small (2.5%) change in maximum radius

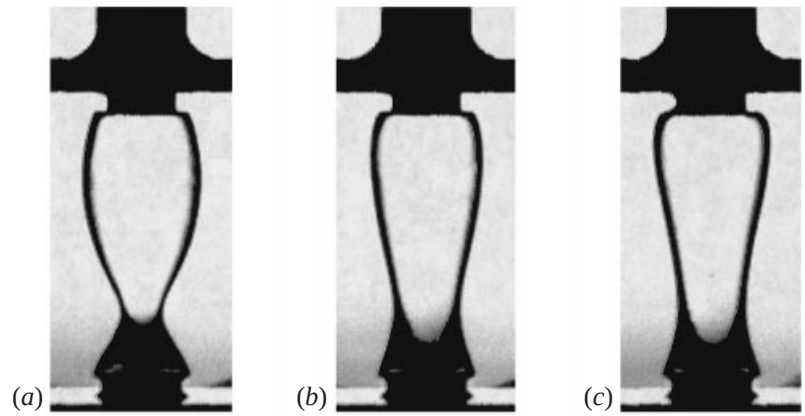

FIGURE 7. Images of a castor oil/eugenol bridge in silicone oil 12 M with increasing fields at $\beta = 3.36$. The electric field parameters are (*a*) $\Delta = 0.0652$, (*b*) $\Delta = 0.1094$, and (*c*) $\Delta = 0.1774$.

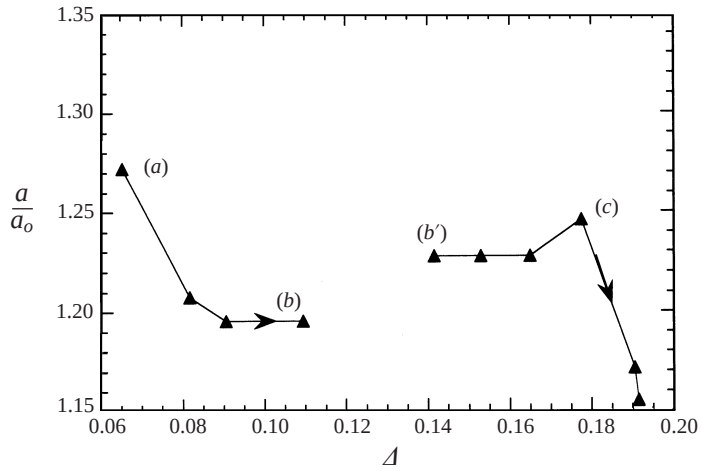

FIGURE 8. Relation between maximum bridge radius and Δ for a castor oil/eugenol bridge in silicone oil 12 M at $\beta = 3.36$. The lettered points correspond to the images in figure 7.

between points (*b*) and (*b*′) arose when the field polarity was reversed twice during a period of a few seconds while simultaneously increasing the field strength (by 12%). This was done simply to put a stress on the system and observe its response. The change in configuration seems to illustrate the presence of a small amount of hysteresis in the 'shape trajectory'. This is not surprising given that the (nonlinear) deformation processes involve a complex balance between electrical, hydrodynamic, and interfacial tension stresses at the interface along with fluid motion inside the deformed bridge.

Sankaran & Saville (1993) noted that in their ground-based experiments the amphora was always oriented with the 'bulge' nearer the positive electrode. According to the leaky dielectric model, the deformation scales with the square of the field strength so the sense of the deformation should be independent of field orientation. Identical, and still unexplained, behaviour was found in the microgravity experiments following a polarity reversal irrespective of which electrode was grounded. Nevertheless, the

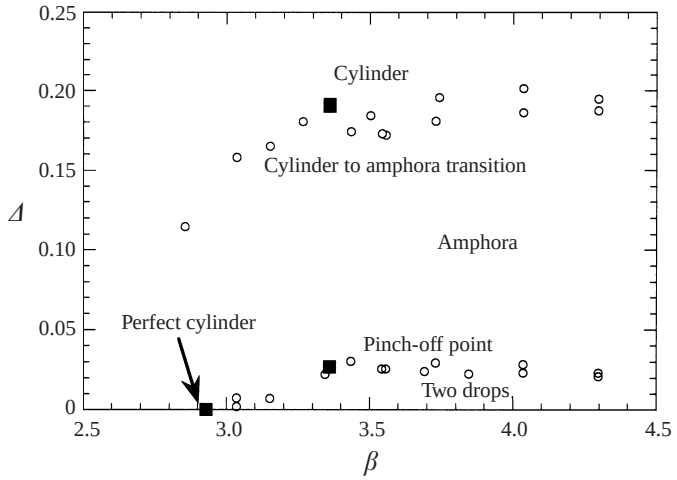

FIGURE 9. Castor oil/eugenol bridges in silicone oil 12 M. Microgravity experiments – filled symbols; terrestrial experiments – open symbols.

shape of the amphora following a change was robust in that changes in the maximum diameter of an amphora following reversal of the field direction were small (less than 5%), about the same as the uncertainty in determining the interface location.

With the two-phase system, the conditions for the amphora–cylinder transition and pinch-off agree with the results of Sankaran & Saville (1993), as shown in figure 9. In the microgravity experiments, the first transition occurred at $\Delta = 0.191$ and the latter at $\Delta = 0.027$; corresponding values reported by Sankaran & Saville are $\Delta = 0.18$ and 0.03.

Figure 9 also illustrates the effectiveness of the microgravity environment compared to small 'matched-density' ground experiments (cf. the point at $\beta = 2.92$, labelled 'perfect cylinder'). Although the Bond number in their experiments was small (4×10^{-3}), Sankaran & Saville (1993) found it necessary to apply an electric field to secure a 'perfect' cylinder at conditions slightly below the Plateau limit because of residual effects of buoyancy. In the microgravity experiments, no field was necessary to maintain a cylinder close to the Plateau point.

Some AC field experiments were carried out with the castor oil–silicone oil cell. Since the shortest electrical relaxation time for the castor oil/eugenol–silicone oil system is 0.02 s (table 1), fields oscillating at frequencies above 100 Hz should be capable of stabilizing the bridge since it will behave as a perfect dielectric (González *et al.* 1989; Sankaran & Saville 1993). With a field oscillating at 200 Hz, an intact (deformed) bridge was formed with $\Delta_{RMS} = 0.48$ and $\beta = 3.54$. This value of Δ_{RMS} is below that computed for the cylinder–amphora transition (2.39) from the perfect dielectric theory of González *et al.* However, this is to be expected since the bridge shape is amphora-like. These results are, therefore, consistent with perfect dielectric behaviour.

5.2. *A castor oil bridge in a dielectric gas, SF_6*

After forming a bridge using the Taylor cone procedure, its behaviour was investigated at aspect ratios of 2.79, and 2.91 (figure 10*a*, *b*). As expected, these configurations were stable without a field. To illustrate the bridges shape sensitivity, a bridge with $\beta = 2.96$ was stretched slightly (by 170 μm) without adding fluid. At this point, the

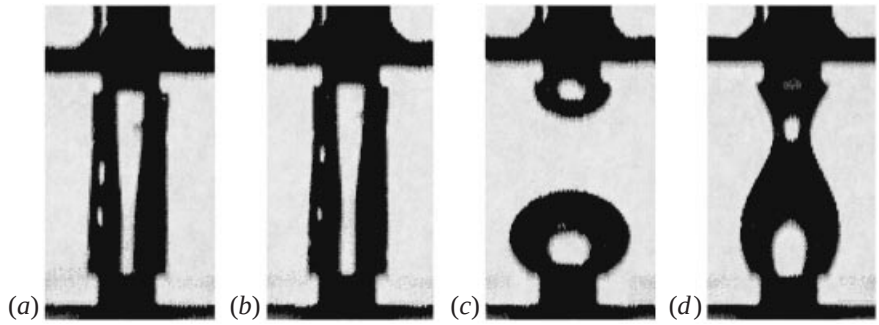

FIGURE 10. Castor oil bridges in SF_6 at (*a*) $\Delta = 0$, $\beta = 2.79$; (*b*) $\Delta = 0$, $\beta = 2.91$; (*c*) $\Delta = 0$, $\beta = 2.96$; and (*d*) $\Delta = 0.140$, $\beta = 2.96$. The positive electrode is at the bottom.

bridge became unstable (figure 10*c*) because it was 'under volume' and the critical aspect ratio for lean bridges is less than π (Boucher & Jones 1998). Upon imposing a field, a stable bridge formed (figure 10*d*).

Bridge behaviour in steady fields was investigated at two aspect ratios: 3.23 and 4.32. Starting from a broken bridge at $\beta = 3.23$ (figures 11 and 12), the electric field was increased incrementally until coalescence occurred at $\Delta = 0.14$. At $\Delta = 0.44$, the amphora–cylinder transition occurred. Then, with a cylindrical bridge established, the polarity was reversed and the field lowered to search for the cylinder–amphora transition (figures 13 and 14). This occurred at $\Delta = 0.26$ – much lower than the amphora–cylinder transition with an increasing field. Pinch-off into two drops was at $\Delta = 0.095$, close to the coalescence value. The sequence of bridge shapes shown in the figures resulted from slow, deliberate changes in field strength. Sufficient time was allowed after a change in the field to ensure that the new shape was steady by inspecting the behaviour of the Fourier coefficients. Two noteworthy features were identified: (i) the presence of hysteresis (cf. figures 12 and 14) and (ii) amphora orientation. After switching polarity with an amphora bridge, the 'bulge' re-positioned itself nearer the positive electrode, as found with the castor oil/eugenol–silicone oil system. The hysteresis is not unexpected, given the differences in the bridge configurations prior to the transition in the two situations. Before the amphora-to-cylinder transition, the electrohydrodynamic flow contributes to the balance of stresses; at the cylinder-to-amphora transition, the cylinder is quiescent until an 'instability' arises to sustain the deformation.

A similar series of experiments was carried out at $\beta = 4.32$. Starting with an amphora shape, the transition to a cylinder occurred $\Delta = 0.94$. The cylinder–amphora transition took place at $\Delta = 0.64$, and pinch-off at $\Delta = 0.35$. Surprisingly, the amphora's bulge was located near the negative electrode – opposite its location at the smaller aspect ratio. The orientation of the bulge is perplexing and such behaviour deserves closer scrutiny.

An interesting dynamic pattern ensued following pinch-off at either aspect ratio. Instead of remaining separated, the opposing drops deformed until the bridge reformed. Then the bridge collapsed (since the field was below that required for an intact bridge) and reformed periodically in the steady field. Figure 15 shows behaviour at $\beta = 4.32$. The oscillation period was 4.8 s and remained so for over ten minutes. Note that the first and last images of the figure are identical. The break-up – re-formation process arises from charge accumulation on the two drops. After the bridge ruptures, charge of opposite sign accumulates on each drop owing to castor oil's conductivity.

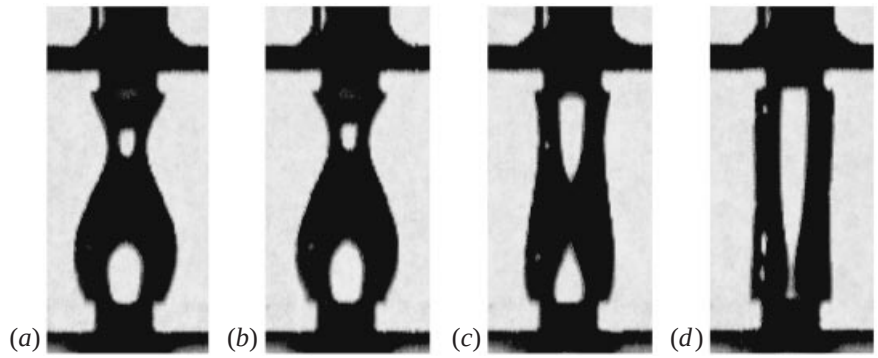

FIGURE 11. Castor oil bridge in SF_6 under increasing electric fields at $\beta = 3.23$. The electric field parameter is: (*a*) $\Delta = 0.1423$, (*b*) $\Delta = 0.2604$, (*c*) $\Delta = 0.4138$, and (*d*) $\Delta = 0.4428$. The positive electrode is at the bottom. Note that the dimensionless maximum radius for the cylinders in figures 12 and 14 is ~ 1.01. Since the radius of the bridge is 2.475 mm, this amounts to a deviation of about 25 μm, well within the calibrated uncertainty due to the size of a pixel. Nevertheless, reconstruction of the interface in these situations (from the image analysis) shows that it is indeed 'cylindrical'.

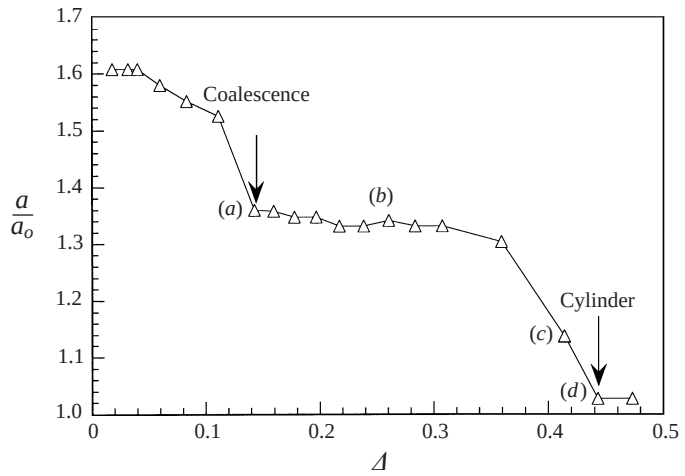

FIGURE 12. Relation between maximum bridge radius and Δ for a castor oil bridge in SF_6 at $\beta = 3.23$. The bridge is broken until point (*a*) where coalescence occurs. At point (*d*), the bridge becomes a perfect cylinder. The labelled points correspond to the images in figure 11.

As charge on the drop surface increases, the drop is pulled towards the opposite electrode where it coalesces with the other drop. When the bridge is re-established, charge leaks off the bridge interface and, since the field is below that required for a stable bridge, it splits apart and the cycle starts anew. The oscillation frequency is consistent with the charge relaxation time, τ_e, defined in (5), and represents the time necessary for charge relaxation. For castor oil the characteristic time is 1.2 s.

Experiments with castor oil bridges in SF_6 in sinusoidal fields yielded unexpected results. Although the castor oil/eugenol–silicone oil bridge could be stabilized in an AC field, the behaviour of castor oil in SF_6 was quite different. After forming a bridge with aspect ratio of 4.32 in a steady field, a sinusoidal potential was applied at the highest voltage available from the power supply ($\Delta_{RMS} = 1.36$), well above the level required to stabilize the bridge according to the theory set out by González *et al.*

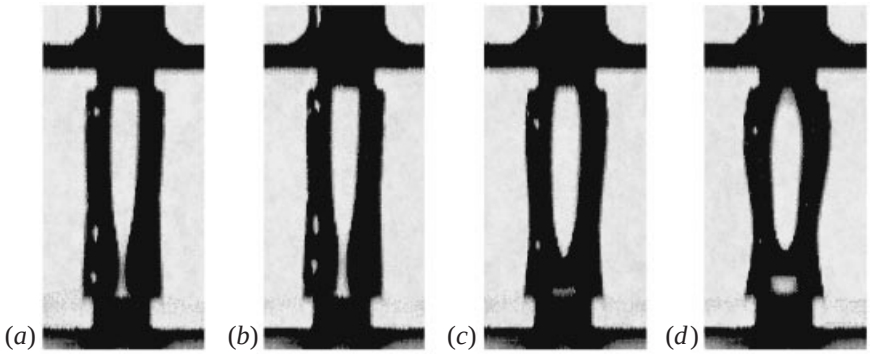

FIGURE 13. Images of a castor oil bridge in SF_6 under decreasing electric fields at $\beta = 3.23$. The electric field parameter is: (*a*) $\Delta = 04138$, (*b*) $\Delta = 0.3325$, (*c*) $\Delta = 0.2374$, and (*d*) $\Delta = 0.0961$. The positive electrode is at the top.

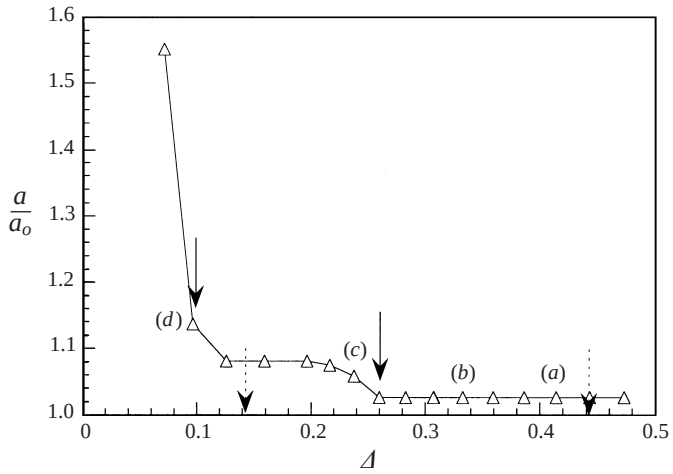

FIGURE 14. Relation between maximum bridge radius and Δ for a castor oil bridge in SF_6 at $\beta = 3.23$. The transition from cylinder to amphora is indicated by the solid arrow on the right, and from amphora to cylinder by the broken arrow on the right. The labelled points correspond to the images in figure 13.

(1989). Nevertheless, although the characteristic frequency for castor oil is a little less than 1 Hz, the bridge could not be stabilized at frequencies ranging from 6.6 Hz to 500 Hz. Even after lowering the aspect ratio to 3.77 a stable bridge could not be maintained in a 30 Hz field with Δ_{RMS} at 1.71. Clearly the behaviour of bridges with gas–liquid interfaces differs from that with liquid–liquid interfaces.

5.3. *An enhanced-conductivity castor oil bridge in a dielectric gas, SF_6*

To investigate the effects of conductivity, an enhanced-conductivity castor oil was used. The enhanced conductivity liquid was formulated by adding a small amount (3.7×10^{-9} moles g^{-1}) of the organic electrolyte tetrabutylammonium-tetraphenylborate to the neat castor oil. This increased its conductivity to 1.67×10^{-9} Siemens m^{-1}, over 40 times the conductivity of pure castor oil. With this fluid, stable bridges were observed without a field below the Plateau limit (at $\beta = 2.25$) and with a DC field at $\beta = 3.23$. At low field strengths the amphora was oriented with its belly near the positive

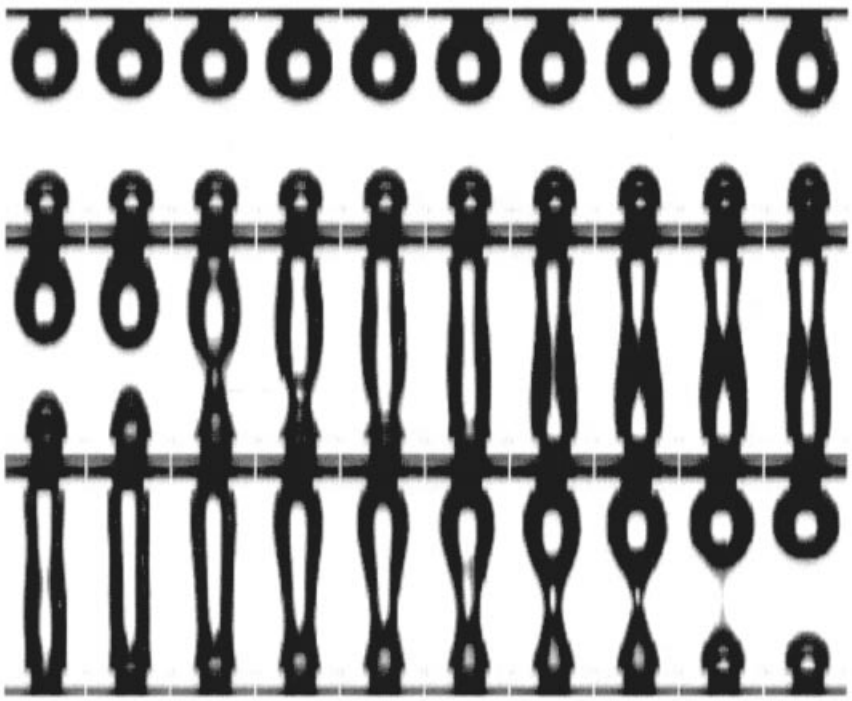

FIGURE 15. A sequence of images taken at 0.17 s intervals showing the periodic reformation and breakup of the bridge at the pinch-off point for a castor oil bridge at $\beta = 4.32$ and $\Delta = 0.3066$. The first and last images are one period apart. The positive electrode is at the bottom.

electrode. The amphora–cylinder transition took place at $\Delta = 0.45$, coinciding with that observed with the low-conductivity castor oil. However, experimentation with the high-conductivity fluid proved difficult and the bridge spilled during attempts to locate the pinch-off condition. Extrapolating the radius–field strength data of pinch-off gave $\Delta = 0.13$, close to that observed with pure castor oil ($\Delta = 0.10$).

To study bridge behaviour in an AC field, spilled fluid was removed by manipulation with the field and pumping. Then a bridge was formed in a DC field with an aspect ratio of 3.41. Although a stable amphora could be maintained at $\Delta = 1.0$, switching to a 200 Hz AC field led to an unstable configuration at $\Delta_{RMS} = 0.74$. The electrical relaxation time for this fluid, 0.024 s, corresponds to a frequency of roughly 40 Hz. According to the perfect dielectric theory, such a bridge should be stable for $\Delta > 0.25$.

5.4. *A silicone oil bridge in a dielectric gas, SF_6*

Another part of the inquiry into the effects of conductivity involved silicone oil 1 M, whose conductivity is less than $\frac{1}{30}$th that of castor oil (table 1). Although stable bridges could be formed without a field at aspect ratios below π, attempts to form a bridge with a DC field at $\beta = 3.22$ were unsuccessful, even with high field strengths (Δ above 3). However, this silicone oil bridge could be stabilized with a 500 Hz field. Here the cylinder–amphora transition occurred at $\Delta_{RMS} = 1.1$ and pinch-off at 0.91. Both are much larger than the theoretical value predicted for the cylinder–amphora transition using the perfect dielectric theory ($\Delta = 0.15$).

6. Summary

Several points deserve further comment. First, many of the observations made in this investigation are consistent with earlier, ground-based experiments and with the leaky dielectric model.

(i) The close agreement between the two-phase experiments in μ-g and terrestrial environments. This indicates that the flight apparatus functioned in a consistent fashion.

(ii) The sustained, periodic oscillation of the castor oil bridge in SF_6. Such behaviour arises from conduction and accumulation of charge. It confirms, as expected, that castor oil behaves as a leaky dielectric.

(iii) The behaviour of high-conductivity castor oil bridges in SF_6 closely mimicked the behaviour of those formed from the lower-conductivity fluid. This is consistent with the leaky dielectric picture where the behaviour of a system with a liquid–gas interface should be independent of the liquid conductivity, cf. (2) and the discussion therafter.

(iv) The sharp, well-defined cylinder-to-amphora transitions. Sharp transitions were observed earlier in terrestrial experiments with isopycnic systems. This behaviour suggests that the transition can be addressed as a linearized, hydrodynamic stability problem. The amphora–cylinder and pinch-off transitions clearly involve nonlinear phenomena and their analysis will be more complex.

Several observations conflict with what is expected with leaky dielectric liquids.

(i) The apparent bias in the orientation of the amphora. In two-phase experiments with castor oil/eugenol mixtures in silicone oil 12 M, the amphora's belly was always located nearest the positive electrode. With castor oil bridges in silicone oil 1 M, the opposite orientation was found. When the polarity was switched, the amphora's orientation followed, showing that the behaviour is not due to apparatus bias. With castor oil in SF_6 the orientation of the amphora changed when the aspect ratio was altered.

With perfect dielectrics the interface polarization charge density is proportional to the field strength normal to the surface. In leaky dielectrics it is the free-charge density that is proportional to the field. Thus, in either case, the stress varies as the square of the field. Accordingly, once an amphora is formed, reversing the field should leave the orientation intact. This behaviour, identified earlier by Sankaran & Saville (1993), is evidence of an apparent shortcoming in the leaky dielectric model as regards the effects of polarity in bridge experiments. Inasmuch as the behaviour is found with liquid–liquid and gas–liquid bridges, it appears to be generic behaviour.

(ii) Unexpected differences between the behaviour of liquids with different conductivities. High- and low-conductivity castor oil bridges could be stabilized in SF_6 with DC fields; they could not be stabilized in AC fields even when the frequency was high enough to nullify free-charge relaxation. Conversely, a very low-conductivity silicone oil bridge could be stabilized in AC but not DC fields.

These experiments involve a 'perfectly reflecting' interface where, according to the leaky dielectric theory, the behaviour should be independent of conductivity in DC fields. Moreover, in AC fields perfect dielectric behaviour should prevail when the frequency is high enough to prevent free-charge accumulation. Since the castor oil bridges could be stabilized in a DC field, similar behaviour should have obtained in AC fields, albeit at a higher field strengths. Because the low-conductivity silicone oil bridge was intact in a strong, high-frequency AC field, it should have remained so

upon reducing the frequency while maintaining the field strength. At present we have no ready explanation for this behaviour.

As noted earlier, conducting research in a microgravity environment by remote control limits the number of experiments and the range of conditions that can be studied. Nevertheless, enough tests were carried out here to ensure that the behaviour is representative and reproducible. It remains to devise configurations where the behaviour of liquid–gas interfaces can be studied more comprehensively.

This work was supported by the National Aeronautics & Space Administration's Microgravity Science and Applications Division and the European Space Agency. As is clear from the text, the contributions of a host of individuals at NASA, ESA, and the various contractors were essential. In addition, we acknowledge the valuable assistance of Dr S. Sankaran, both in the initial stages of this work and with mission operations.

REFERENCES

Boucher, E. A. & Jones, T. G. J. 1988 Equilibrium and stability characteristics of zero-gravity fluid bridges constrained between equal solid rods. *J. Colloid Interface Sci.* **126**, 469–481.

Burcham, C. L. 1998 The electrohydrodynamic stability of a leaky dielectric liquid bridge in an axial electric field with zero Bond number. PhD Thesis, Princeton University.

Feng, J. Q. & Scott, T. C. 1996 A computational analysis of electrohydrodynamics of a leaky dielectric drop in an electric field. *J. Fluid Mech.* **311**, 289–326.

González, H. & Castellanos, A. 1993 The effect of residual gravity on the stability of liquid columns subjected to electric fields. *J. Fluid Mech.* **249**, 185–206.

González, H., McCluskey, F. M. J., Castellanos, A. & Barrero, A. 1989 Stabilization of dielectric liquid bridges by electric fields in the absence of gravity. *J. Fluid Mech.* **206**, 545–561.

Plateau, J. 1863 Experimental and theoretical researches on the figures of equilibrium of a liquid mass withdrawn from the action of gravity, etc. *Annual Report of the Board of Regents of the Smithsonian Institution*, Pt. 1, House of Representatives Misc. Doc. #83, 38th Congress, 1st Session, pp. 207–285.

Plateau, J. 1864 Experimental and theoretical researches on the figures of equilibrium of a liquid mass withdrawn from the action of gravity, etc. *Annual Report of the Board of Regents of the Smithsonian Institution*, Pts. 2–4, House of Representatives Misc. Doc. #54, 38th Congress, 2nd Session, pp. 285–369.

Plateau, J. 1865 Experimental and theoretical researches on the figures of equilibrium of a liquid mass withdrawn from the action of gravity, etc. *Annual Report of the Board of Regents of the Smithsonian Institution*, Pt. 5, House of Representatives Misc. Doc. #102, 39th Congress, 2nd Session, pp. 411–435.

Plateau, J. 1866 Experimental and theoretical researches on the figures of equilibrium of a liquid mass withdrawn from the action of gravity, etc. *Annual Report of the Board of Regents of the Smithsonian Institution*, Pt. 6, House of Representatives Misc. Doc. #83, 39th Congress, 2nd Session, pp. 255–289.

Pletser, V. 1997 The bubble, drop, particle unit on Spacelab LMS. Nominal and troubleshooting operations. *Acta Astro.* **40**, 639–654.

Pletser, V., Burcham, C. L. & Cronise, R. 1995 A BDPU Preparatory experiment for Spacelab LMS during parabolic flights with NASA-LeRC DC-9 aircraft. *Microgravity News from ESA* **8**, 3, 4–10.

Press, W. H., Teukolsky, S. A., Vetterling, W. T. & Flannery, B. P. 1992 *Numerical Recipes*, 2nd Edn. Cambridge University Press.

Ramos, A. & Castellanos, A. 1993 Bifurcation diagrams of axisymmetric liquid bridges of arbitrary volume in electric and gravitational axial fields. *J. Fluid Mech.* **249**, 207–225.

Ramos, A., González, H. & Castellanos, A. 1994 Experiments on dielectric liquid bridges subjected to axial electric fields. *Phys. Fluids* **6**, 3206–3208.

Sankaran, S. & Saville, D. A. 1993 Experiments on the stability of a liquid bridge in an axial electric field. *Phys. Fluids* **5**, 1081–1083.

Saville, D. A. 1997 Electrohydrodynamics: The Taylor-Melcher leaky dielectric model. *Ann. Rev. Fluid Mech.* **29**, 27–64.

Taylor, G. I. 1966 Studies in electrohydrodynamics. I. The circulation produced in a drop by an electric field. *Proc. R. Soc. Lond.* A **291**, 159–166.

Torza, S., Cox, R. G. & Mason, S. G. 1971 Electrohydrodynamic deformation and burst of liquid drops. *Phil. Trans. R. Soc. Lond.* A **269**, 295–319.

Vizika, O. & Saville, D. A. 1992 The electrohydrodynamic deformation of drops suspended in liquids in steady and oscillatory fields. *J. Fluid Mech.* **239**, 1–16.

Zhang, X., Padgett, R. S. & Basaran, O. A. 1996 Nonlinear deformation and breakup of stretching liquid bridges. *J. Fluid Mech.* **329**, 207.